UDK 669.15’24’25-196:66.011
Original scientific article/Izvirni znanstveni članek

ISSN 1580-2949
MTAEC9, 56(5)515(2022)

CORRECTION OF FLOW CURVES AND CONSTITUTIVE MODELING OF AN AS-CAST N06625 NICKEL-BASED ALLOY

KOREKCIJA KRIVULJ TEČENJA IN KONSTITUTIVNO MODELIRANJE LITE NIKLJEVE ZLITINE N06625

Shuo Yang[1], Yugui Li[1,2*], Yaohui Song[1], Bin Wang[1], Yuewu Zheng[1], Xiaobiao Liu[1], Yao Li[1]

[1]School of Materials Science and Engineering, Taiyuan University of Science and Technology, Taiyuan, China
[2]School of Mechanical Engineering, Taiyuan University of Science and Technology, Taiyuan, China

Prejem rokopisa – received: 2022-05-11; sprejem za objavo – accepted for publication: 2022-08-01

doi:10.17222/mit.2022.496

On a Gleeble-3800 simulator, isothermal hot compression tests of an as-cast N06625 nickel-based alloy were conducted in a wide range of temperatures (950–1200 °C) and strain rates (0.1–50 s^{-1}). Considering the influence of friction and adiabatic heating in the test, the flow curves were corrected. A modified Johnson-Cook, strain-compensated Arrhenius-type and modified Hensel-Spittel constitutive models were established based on the corrected flow curves. In a hot compression test, the flow stress is mainly affected by the coupling of the temperature, strain rate and strain, so the consideration of the coupling effect greatly affects the accuracy of the constitutive model. Moreover, different materials have different sensitivities to the three conditions. Therefore, the improved model in this paper can improve its universality and accuracy after adding relevant parts to it. The models were compared using the correlation coefficient (R) and average absolute relative error (AARE) to determine their accuracy in predicting the deformation behavior of the above alloy. According to our findings, the strain-compensated Arrhenius-type model provided the greatest forecast accuracy over the whole temperature and strain rate range. Under a certain temperature and strain rate, the modified Johnson-Cook model provided the best prediction accuracy.

Keywords: alloy N06625, modification, stress-strain curve, constitutive model

Avtorji so izvajali izotermne tlačne preizkuse na litini Ni vrste N06625 s simulatorjem Gleeble-3800 v temperaturnem območju med 950 °C in 1200 °C in pri hitrostih deformacije med 0,1 s^{-1} in 50 s^{-1}. Ob upoštevanju vpliva trenja in adiabatnega segrevanja med preizkusi so izvedli korekcije krivulj tečenja. Na osnovi korigiranih krivulj tečenja so določili modele: model po Johnson-Cooku, deformacijsko kompenziran model Arrheniusovega tipa in modificiran Hensel-Spittel konstitutivni model. Med vročimi tlačnimi preizkusi je bila predvsem napetost tečenja odvisna od kombinacije temperature, hitrosti deformacije in deformacije, kar je močno vplivalo na točnost konstitutivnega modela. Zavedati se moramo, da so različni materiali različno občutljivi na vsa tri stanja. Zato lahko izboljšan model, ki je predstavljen, postane univerzalen pristop in tako tudi bolj natančen model za druge materiale, seveda z dodatkom ustreznih parametrov. Izdelane modele so avtorji medsebojno primerjali z uporabo korelacijskega koeficienta (R) in povprečne absolutne relativne napake (AARE; angl.: average absolute relative error). S tem so določili njihovo natančnost napovedi z realno deformacijo izbrane zlitine. Na osnovi raziskav ugotavljajo, da deformacijsko kompenziran model Arrheniusovega tipa zagotavlja najboljšo natančnost v celotnem temperaturnem območju in pri vseh izbranih hitrostih deformacije. Pri določeni temperaturi in hitrosti deformacije, izbiri ene same krivulje tečenja, pa Johnson-Cookov model zgotavlja najboljšo natančnost napovedi.

Ključne besede: zlitina N06625, modifikacija, krivulja napetost-deformacija, konstitutivni model

1 INTRODUCTION

The N06625 nickel-based alloy is a Ni-Cr solid solution strengthened nickel-based alloy with Mo and Nb as the major strengthening elements. Although it is a solid solution strengthened alloy, depending upon the Nb and C percentages, there could be a development of second-phase particles such as γ and carbides at particular aging conditions.[1–3] The alloy is extensively used in aeronautic, aerospace, chemical, nuclear, petrochemical and marine applications due to its good mechanical properties, and resistance to high-temperature corrosion and damage after prolonged exposure to aggressive environments.[3–5]

The flow behavior of metals and alloys during thermal deformation is a complex and comprehensive interaction of many factors. During hot deformation, the strain rate, strain and forming temperature affect the microstructure evolution, while the mechanical properties are affected by the microstructure evolution.[6,7] The study of the high-temperature flow behavior of alloys is of great help to designers in formulating a reasonable hot-working process.

At present, finite-element simulation software has occupied an irreplaceable position in the actual production process, and the accuracy of simulation results also greatly affects the quality of production. A constitutive model is the core of a finite-element simulation. Choosing the appropriate constitutive model can significantly improve the prediction accuracy of the simulation. Many scholars have developed various constitutive mod-

*Corresponding author's e-mail:
liyugui@tyust.edu.cn (Yugui Li)

Table 1: Chemical composition of the N06625 nickel-based alloy (*w*/%)

Ni	Cr	Mo	Nb	Fe	Co	Si	Mn	Ti	Al	C	Cu	S	P
≥ 58	20–30	8–10	3.15–4.15	≤ 5	≤ 1	≤ 0.5	≤ 0.5	≤ 0.4	≤ 0.4	≤ 0.1	≤ 0.07	≤ 0.015	≤ 0.015

els and their improved models.[6] Among these models, the Johnson-Cook model and the Arrhenius model are widely used for metals and alloys. Badrish[8] carried out a tensile test with Inconel 625 and established the JC-ZA model. The applicability of the model to Inconel 625 was proved by using a variety of statistical parameters. Godasu[9] found that the Arrhenius model can accurately reflect the high-temperature deformation mechanical properties of superalloy 625. Gupta[10] established the Johnson-Cook, a modified Zerilli-Armstrong, a modified Arrhenius-type, and the ANN models of austenitic stainless steel 316. The correlation coefficient of the ANN model is the highest (0.9930). But due to its difficulty in integrating with the finite-element modeling software and the fact that it is a black-box model, constitutive equations have generally been given a higher preference over ANN. Brown[11] established seven types of constitutive models. Taken together, the modified Johnson-Cook, Zener-Hollomon, Hensel-Spittel and modified Hensel-Spittel models provide the best fit with the experimental results. Cai[12] developed a modified Johnson-Cook and strain-compensated Arrhenius-type model of different phase regimes. The results indicated that the accuracy of the modified Johnson-Cook model is higher than that of the strain-compensated Arrhenius-type model at the $\alpha + \beta$ phase. Meanwhile, the time required for evaluating the material constants of the modified Johnson-Cook model is much shorter than that of the strain-compensated Arrhenius-type model. Although these studies are available, limited literature shows a comparison of different constitutive models related to the N06625 nickel-base alloy.

The data of a constitutive model are mostly based on isothermal compression tests. In a thermal compression test, there is usually some error in the final stress-strain curve, which is limited by the test conditions. The error mainly comes from two aspects: one is the influence of friction on the flow stress, and the other is the influence of deformation temperature rise on the flow stress.[13]

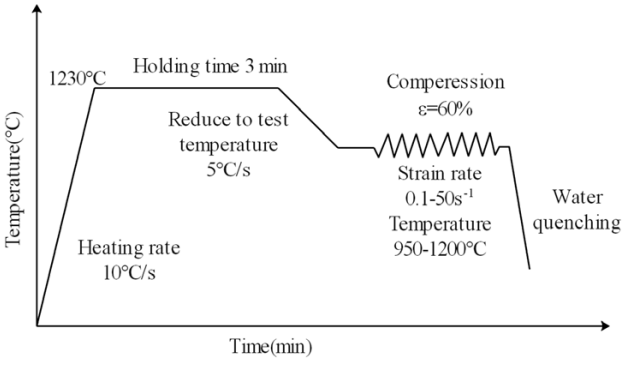

Figure 1: Hot-compression test process

Therefore, many scholars propose to modify the flow stress according to these two factors.

The purpose of this study was to develop a constitutive model suitable for the high-temperature flow behavior of the as-cast N06625 nickel-based alloy. Therefore, isothermal compression tests were carried out in a wide range of temperatures and strain rates. The flow curve was modified to consider the effects of friction and temperature rise. Then the coefficients of various constitutive models were determined using the modified data. Finally, the correlation coefficient and average absolute relative error were used to examine the validity of the constitutive equations over the entire range of temperatures and strain rates, and the prediction capabilities of the three constitutive models were compared.

2 EXPERIMENTAL PART

The material used in the test is an N06625 nickel-based alloy ingot. Its chemical composition is shown in **Table 1**. A hot-compression test sample is prepared by a wire-cut electrical discharge machine 15 mm away from the edge of the ingot to ensure the consistency of the grain of the hot-compression simulation sample. The samples are cylinders with a diameter of ϕ 10 mm and a length of 15 mm.

Constant-temperature and constant-strain-rate thermal-compression simulation tests are carried out on a Gleeble-3800 simulation machine. During the tests, a graphite lubricant is applied on both ends of a sample and tantalum sheets are used to help reduce friction and avoid adhesion between a sample and the equipment. The samples are heated to the preset temperature at a heating rate of 10 °C/s and held at it for 3 min to obtain uniform and equiaxed grains. The samples are then cooled down to (950, 1000, 1050, 1100, 1150 and 1200) °C at a cooling rate of 5 °C/s. The samples are compressed by 60 % at strain rates of (0.1, 1, 10 and 50) s^{-1}, and cooled rapidly after the deformation.

3 RESULTS AND DISCUSSION

3.1 Correction of the stress-strain curve

The flow stress requires friction and temperature corrections during deformation. The stress after friction correction is:[14,15]

$$\sigma_f = \frac{P(2\mu R/h)^2}{2\left[\exp(2\mu R/h) - 2\mu R/h - 1\right]} \quad (1)$$

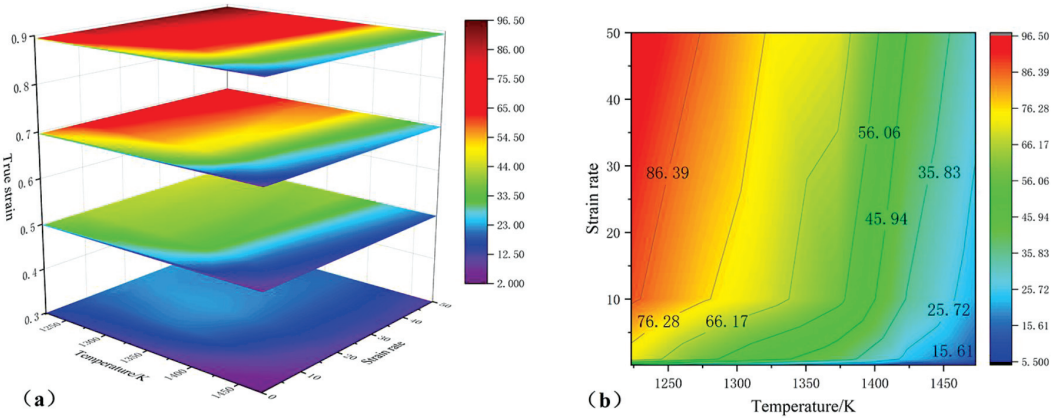

Figure 2: Temperature changes of the samples under different deformation conditions: a) ε = 0.3–0.9, b) ε = 0.9

$$\mu = \frac{\frac{R_1}{H_1} b}{\frac{4}{\sqrt{3}} - \frac{2b}{3\sqrt{3}}} \tag{2}$$

$$b = 4 \frac{\Delta R}{R_1} \cdot \frac{h_1}{\Delta h_1} \tag{3}$$

$$R_1 = R_0 \sqrt{H_0 / H_1} \tag{4}$$

Here, σ_f is the friction-corrected flow stress, P is the uncorrected flow stress, R and h are the momentary radius and height of a sample, respectively, μ is the friction coefficient, b is the barrel parameter, R_1 is the average radius of the cylinder after deformation, ΔR is the difference between the maximum and top radius of the cylinder, H_0 is the initial height of the cylinder, H_1 is the final height, and ΔH_1 is the difference between the initial and final heights of a specimen.

The adiabatic-temperature rise during deformation can be calculated using the following Equation (5):[16]

$$\Delta T = \frac{0.95\eta}{\rho C} \int_0^{\varepsilon} \sigma_f \, d\varepsilon \tag{5}$$

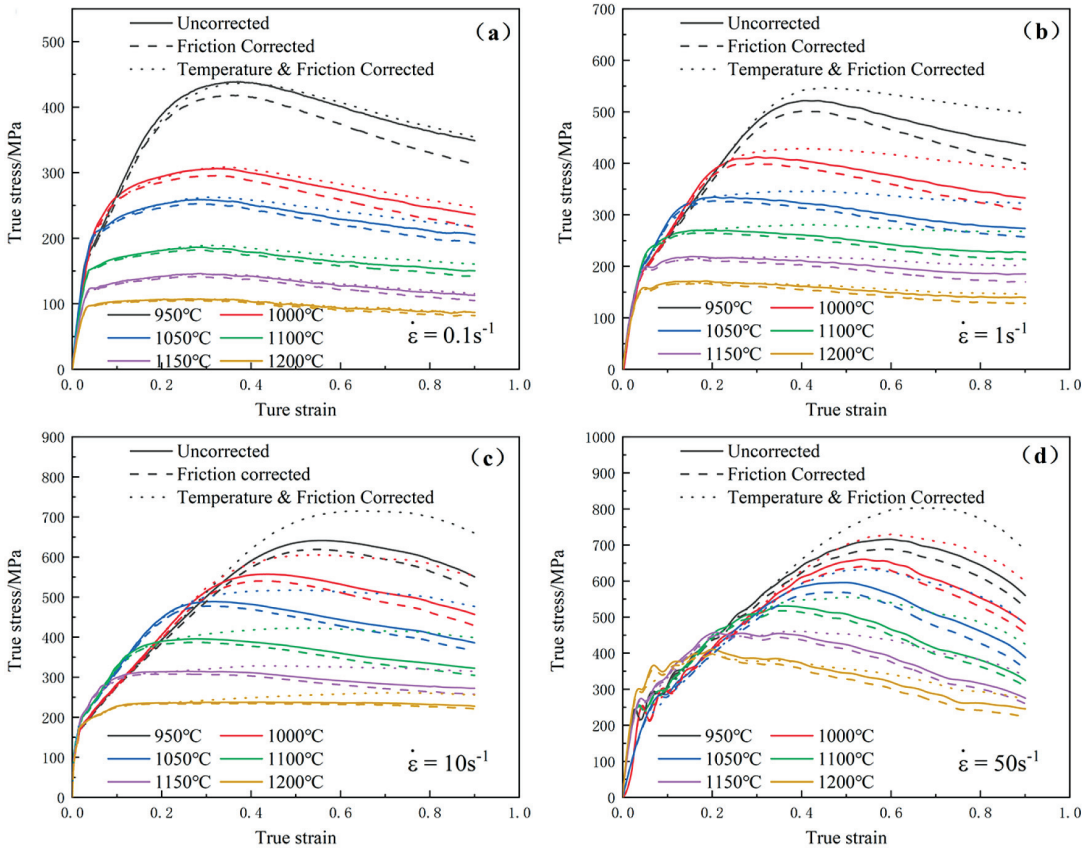

Figure 3: Comparison between the corrected and uncorrected true stress-strain curves: a) 0.1 s^{-1}, b) 1 s^{-1}, c) 10 s^{-1}, d) 50 s^{-1}

where ΔT is the temperature change, ρ is the material density, C_p is the heat capacity and η is the adiabatic factor.[17]

$$\eta = \begin{cases} 0 & \dot{\varepsilon} \le 0.001\ \mathrm{s}^{-1} \\ 0.316 \lg \dot{\varepsilon} + 0.95 & 0.001\ \mathrm{s}^{-1} < \dot{\varepsilon} < 1\ \mathrm{s}^{-1} \\ 0.95 & \dot{\varepsilon} \ge 1\ \mathrm{s}^{-1} \end{cases} \quad (6)$$

The temperature change increases with an increasing strain, as shown in **Figure 2a**, due to the accumulation of adiabatic-temperature rise and friction. The influence of the heat generated by deformation on the temperature change gradually decreases as deformation temperature increases, as shown in **Figure 2b**. This is because the lower the deformation temperature, the higher is the rheological stress value. More external energy is required to achieve the same deformation degree, which means that more energy is dissipated in the form of heat, and the temperature-rise phenomenon becomes more obvious.

Figure 3 shows the original and corrected stress-strain curves under different deformation conditions. The shape of the curve is related to the temperature and strain rate, and the maximum flow stress decreases as the temperature and strain rate increase.

At the same time, it should be noted that at lower strain rates and higher temperatures, the difference between the corrected and uncorrected flow stresses is not significant. However, this difference is no longer negligible at higher strain rates and lower temperatures.

3.2 Constitutive model

3.2.1 Modified Johnson-Cook constitutive model

Lin[18] proposed a modified Johnson-Cook model considering the interaction of the strain rate and temperature:

$$\sigma = \left[A_0 + A_1\varepsilon + A_1\varepsilon^2 + A_1\varepsilon^3\right]\left[1 + C\ln\left(\frac{\dot{\varepsilon}}{\dot{\varepsilon}_0}\right)\right] \cdot \left[\exp\left\{\left[m_1 + m_2\ln\left(\frac{\dot{\varepsilon}}{\dot{\varepsilon}_0}\right)\right](T - T_0)\right\}\right] \quad (7)$$

where A_0, A_1, A_2, A_3, m_1 and m_2 are the material constants.

950 °C and 1 s^{-1} are selected as the reference temperature and strain rate. Under the reference temperature and strain rate, Equation (7) can be simplified to Equation (8). The values of A_0, A_1, A_2 and A_3 can be obtained by fitting σ and ε with third-order polynomials.

$$\sigma = A_0 + A_1\varepsilon + A_1\varepsilon^2 + A_1\varepsilon^3 \quad (8)$$

At the reference temperature, Equation (7) can be simplified to Equation (9). The average slope obtained

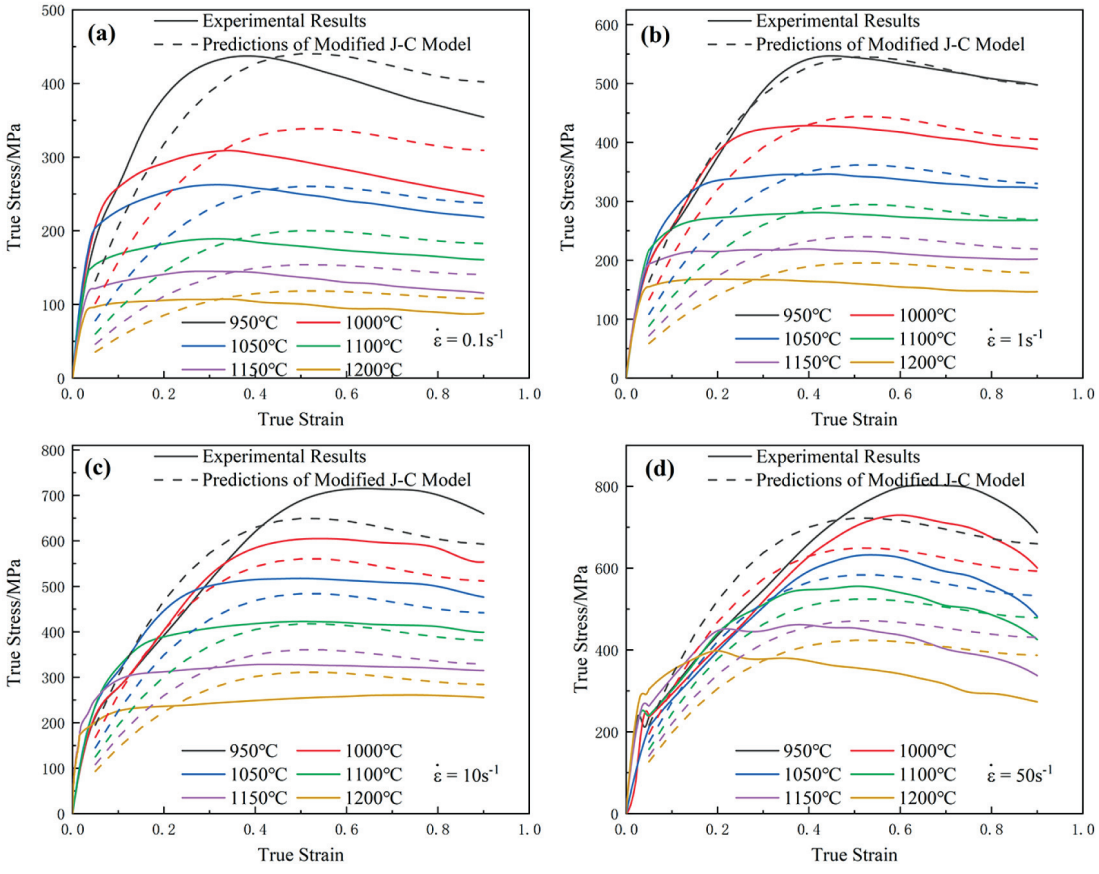

Figure 4: Comparison of the predicted and tested values of the modified Johnson-Cook constitutive model: a) 0.1 s^{-1}, b) 1 s^{-1}, c) 10 s^{-1}, d) 50 s^{-1}

with the linear fitting of ln# and $\sigma/(A_0+A_1\varepsilon+A_2\varepsilon^2+A_3\varepsilon^3)$ is the value of C.

$$\sigma = \left[A_0 + A_1\varepsilon + A_1\varepsilon^2 + A_1\varepsilon^3\right]\left[1 + C\ln\left(\frac{\dot{\varepsilon}}{\dot{\varepsilon}_0}\right)\right] \quad (9)$$

Equation (7) can be converted and natural logarithms taken on both sides. The slopes of $\ln\{\sigma/[(A_0 + A_1\varepsilon + A_2\varepsilon^2 + A_3\varepsilon^3)[1 + C\ln(\dot{\varepsilon}/\dot{\varepsilon}_0)]]\}$ and $(T–T_0)$ are solved under different conditions, then the slopes and $\ln(\dot{\varepsilon}/\dot{\varepsilon}_0)$ are linearly fitted to obtain the values of m_1 and m_2.

$$\ln\left\{\frac{\sigma}{(A_0 + A_1\varepsilon + A_1\varepsilon^2 + A_1\varepsilon^3)\left[1 + C\ln\left(\frac{\dot{\varepsilon}}{\dot{\varepsilon}_0}\right)\right]}\right\} = \quad (10)$$

$$= \left[m_1 + m_2\ln\left(\frac{\dot{\varepsilon}}{\dot{\varepsilon}_0}\right)\right](T - T_0)$$

So far, the parameters of the modified Johnson-Cook constitutive model have been solved.

3.2.2 Strain-compensated Arrhenius-type constitutive model

The Arrhenius constitutive model is shown in Equation (11).[19] So far, the Arrhenius model and improved model have been the most widely used.

$$\dot{\varepsilon} = \begin{cases} A_1\sigma^{n_1}\exp\left(-\dfrac{Q}{RT}\right) & \alpha\sigma \le 0.8 \\ A_2\exp(\beta\sigma)\exp\left(-\dfrac{Q}{RT}\right) & \alpha\sigma \ge 1.2 \\ A[\sinh(\alpha\sigma)]^n\exp\left(-\dfrac{Q}{RT}\right) & \text{for all } \sigma \end{cases} \quad (11)$$

Here, Q is the thermal activation energy and R is the standard molar gas constant.

Some scholars use the Zener-Hollomon parameters to further characterize the model:[20]

$$Z = A[\sinh(\alpha\sigma)]^n = \dot{\varepsilon}e^{-\frac{Q}{RT}} \quad (12)$$

$$\sinh(\alpha\sigma) = \left(\frac{Z}{A}\right)^{\frac{1}{n}} \quad (13)$$

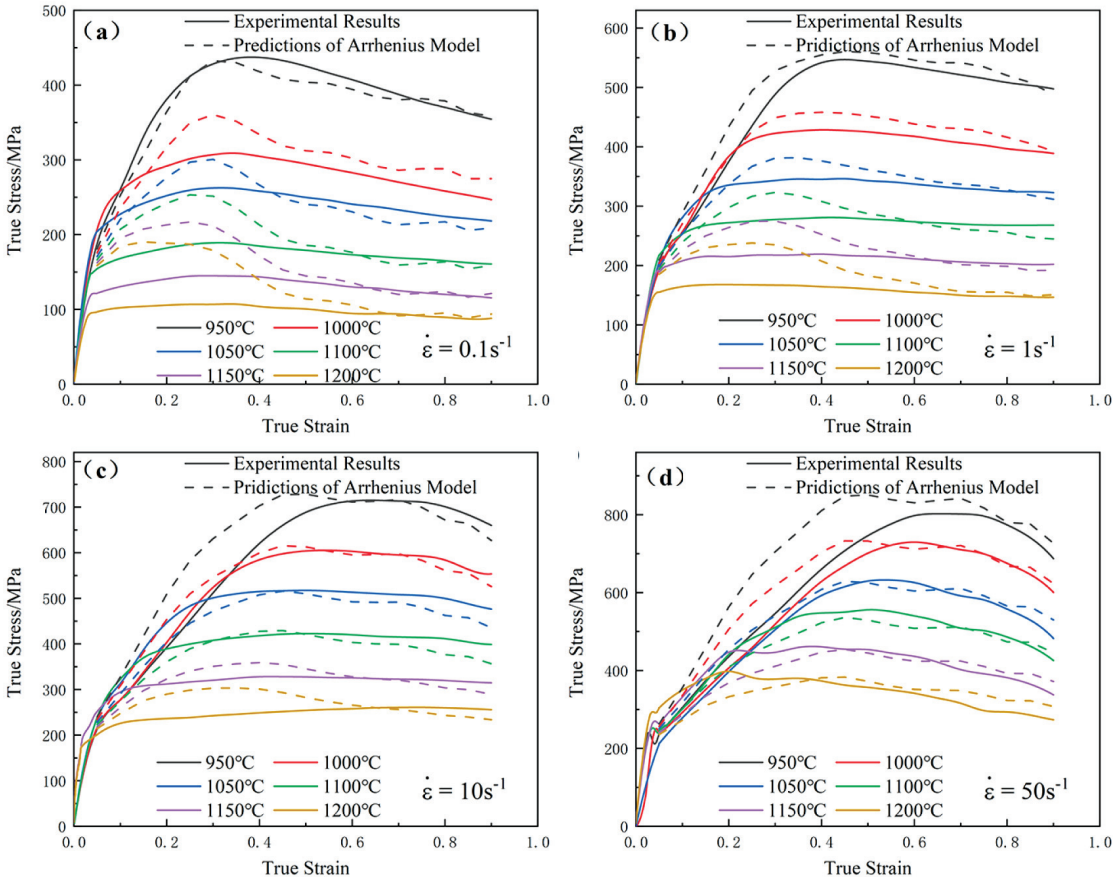

Figure 5: Comparison of the predicted and tested values of the strain-compensated Arrhenius-type constitutive model: a) 0.1 s^{-1}, b) 1 s^{-1}, c) 10 s^{-1}, d) 50 s^{-1}

$$\sigma = \frac{1}{\alpha} \ln\left\{\left(\frac{Z}{A}\right)^{\frac{1}{n}} + \left[\left(\frac{Z}{A}\right)^{\frac{2}{n}} + 1\right]^{\frac{1}{2}}\right\} \tag{14}$$

The following results can be obtained by taking natural logarithms on both sides of Equation (11).

$$\ln \dot{\varepsilon} = \ln A_2 + \beta\sigma - \frac{Q}{RT} \tag{16}$$

$$\ln \dot{\varepsilon} = \ln A + n \ln[\sinh(\alpha\sigma)] - \frac{Q}{RT} \tag{17}$$

Linear fitting is carried out on $\ln \dot{\varepsilon} - \ln \sigma$ and $\ln \dot{\varepsilon} - \sigma$, the average slopes are the values of n_1 and β, respectively. The value of α can be obtained from $\alpha = \beta/n_1$.

We can substitute α into Equation (17) and then perform linear fitting on $\ln \dot{\varepsilon} - \ln[\sinh(\alpha\sigma)]$. The average slope is n and the average intercept is $\ln A - Q/RT$.

$$\ln[\sinh(\alpha\sigma)] = \frac{\ln \dot{\varepsilon}}{n} + \frac{Q}{nRT} - \frac{\ln A}{n} \tag{18}$$

The value of Q can be obtained from Equation (18).

So far, the parameters have been obtained. The flow stress also transforms significantly with the change in the strains; thus, it is necessary to calculate the flow stress in a strain range of 0.05–0.9 at intervals of 0.05. Since the parameters do not correlate, it is necessary to fit their polynomials as a function of strain. Comparing the accumulative error values fitted by polynomials of different times of each parameter, it is found that the accumulative error of the polynomial function of 9 times is minor.

So far, the parameters of the strain-compensated Arrhenius-type constitutive equation have been solved.

3.2.3 Modified Hensel-Spittle constitutive model

The Hensel-Spittel model is a constitutive model with many parameters, proposed by Hensel and Spittel.[21] Spigarelli and El Mehtedi[22] think that this model is not inherently sufficient to describe the change in the strain rate sensitivity at a given temperature and strain. Therefore, some scholars put forward a modified Hensel-Spittel model with the Garofalo equation.[11]

$$\sinh(\alpha\sigma) = A e^{m_1 T} \varepsilon^{m_2} \dot{\varepsilon}^{m_3} e^{m_4/\varepsilon} (1+\varepsilon)^{m_5 T} e^{m_6 \varepsilon} \tag{19}$$

$$\dot{\varepsilon} \exp\left(-\frac{Q}{RT}\right) = A_1 \sigma^{n_1}, \quad \text{for } \alpha\sigma < 0.8 \tag{20}$$

$$\dot{\varepsilon} \exp\left(-\frac{Q}{RT}\right) = A_2 \exp(\beta\sigma), \quad \text{for } \alpha\sigma < 0.8 \tag{21}$$

We take the natural logarithms on both sides of Equation (20) and Equation (21). The values of n_1 and β are

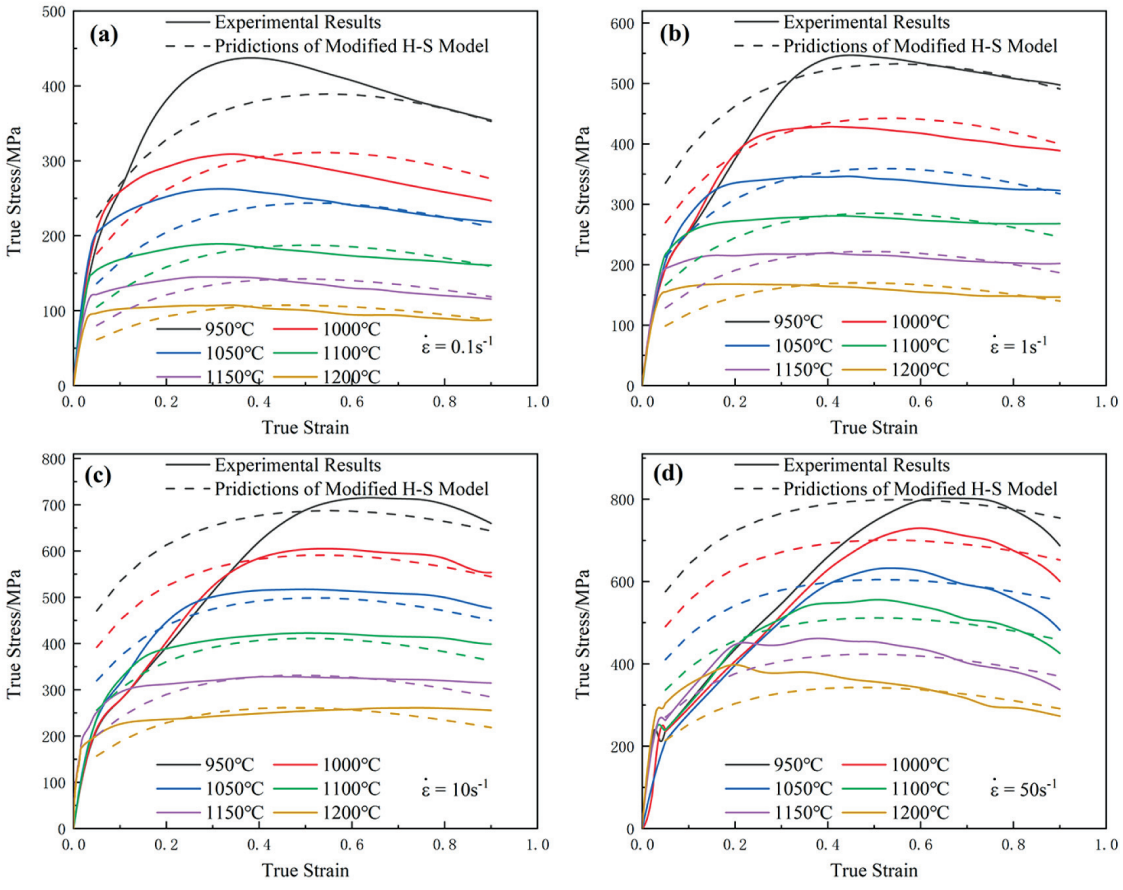

Figure 6: Comparison of the predicted and tested values of the modified Hensel-Spittel model: 0.1 s^{-1}, b) 1 s^{-1}, c) 10 s^{-1}, d) 50 s^{-1}

obtained by linearly fitting $\ln\dot{\varepsilon} - \ln\sigma$ and $\ln\dot{\varepsilon} - \sigma$, respectively. The value of α can be obtained from $\alpha = \beta/n_1$.

$$\ln\dot{\varepsilon} = \ln A_1 + n_1 \ln\sigma - \frac{Q}{RT} \tag{22}$$

$$\ln\dot{\varepsilon} = \ln A_2 + \beta\sigma - \frac{Q}{RT} \tag{23}$$

The strain and strain rate are assumed to be constant. We take the natural logarithms on both sides of Equation (19) at the same time:

$$\ln[\sinh(\alpha\sigma)] = c_1 + [m_1 + m_5 \ln(1+\varepsilon)]T \tag{24}$$

The slope obtained with linear fitting is the value of $m_1 + m_5 \ln(1 + \varepsilon)$. The $m_1 + m_5 \ln(1 + \varepsilon)$ was fitted with $y = p_1 + p_2 \ln(1 + x)$ at a constant strain rate. The values of m_1 and m_5 correspond to the values of p_1 and p_2, respectively.

The strain and temperature are assumed to be constant. We take the natural logarithms on both sides of Equation (19) at the same time:

$$\ln[\sinh(\alpha\sigma)] = c_2 + m_3 \ln\dot{\varepsilon} \tag{25}$$

The slope obtained by linearly fitting $\ln[\sinh(\alpha\sigma)] - \ln\dot{\varepsilon}$ is the value of m_3.

The strain rate and temperature are assumed to be constant. We take the natural logarithms on both sides of Equation (19) at the same time:

$$\ln[\sinh(\alpha\sigma)] = c_3 + m_2 \ln\varepsilon + m_4/\varepsilon + m_5 T \ln(1+\varepsilon) + m_6\varepsilon \tag{26}$$

Equation (26) is fitted with $y = c_3 + m_2\ln x + m_4/x + m_5 T \ln(1 + x)$ to obtain the values of m_2, m_4 and m_6. The currently calculated coefficient is substituted into Equation (19) to obtain the value of A under different conditions. When drawing the A-strain curve, it is found that the value of A is less affected by the temperature and strain rate and more affected by strain. Therefore, the value of A is transformed into a cubic polynomial about the strain, and the value of A and the strain are fitted with a cubic polynomial. So far, all the parameters of the model are obtained.

3.2.4 Comparisons of constitutive models

R and AARE are introduced to evaluate the prediction accuracy of the models.

$$R = \frac{\sum_{i=1}^{N}(E_i - \overline{E})(P_i - \overline{P})}{\sqrt{\sum_{i=1}^{N}(E_i - \overline{E})^2 \sum_{i=1}^{N}(P_i - \overline{P})^2}} \tag{27}$$

$$ARE(\%) = \frac{1}{N}\sum_{i=1}^{N}\left|\frac{(E_i - P_i}{E_i}\right| \times 100\% \tag{28}$$

The average values of R of different models are shown in **Table 2**. **Figure 7** shows the correlation between the test stress and predicted stress of different models. Among the models with strong prediction correlation, the data points closer to the regression line are the most.

Table 2: Comparison of the constitutive models using R

Constitutive model	The average value of R
MJC	0.9533
SA	0.9771
MHS	0.9334

Although R can represent the linear correlation between the experimental value and predicted value, it is not necessarily true that a higher value of R indicates a better result. Therefore, AARE is introduced to further determine the accuracy of the models.

The average values of AARE of different models are shown in **Figure 3**. Contour maps were drawn using the AARE values of each model (**Figure 8**). The AARE values of each model at different strain rates and deformation temperatures are shown in **Figure 8**.

The modified Johnson-Cook model's value of R is 0.9533, and the AARE values range from 2.30 to 25.71. Lin[18] chose a quadratic polynomial in the formula for the modified Johnson-Cook constitutive model for high-strength alloy steel because the curve had the highest fitting degree with the quadratic polynomial. The flow curve of the N06625 nickel-based alloy is more in line with the trend of the third-order polynomial under reference conditions. As a result, Equation (7) has a cubic polynomial. The modified Johnson-Cook constitutive

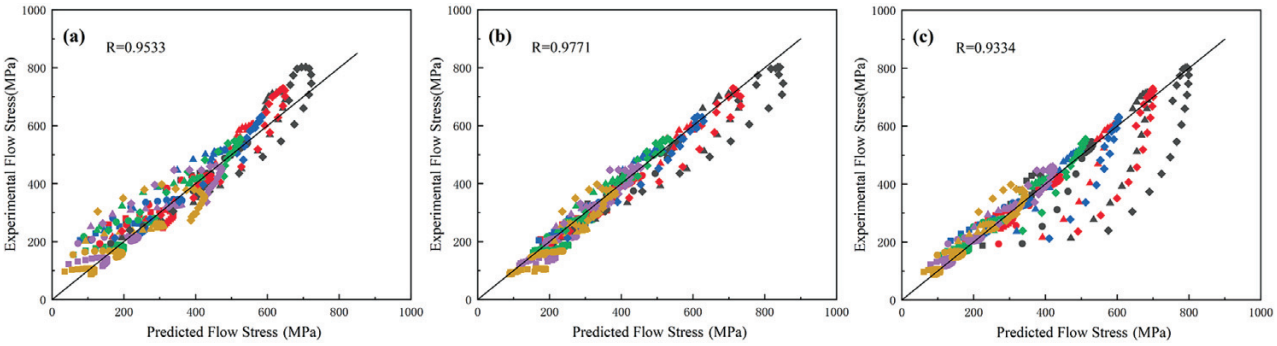

Figure 7: Comparison of R for: a) modified Johnson-Cook, b) strain-compensated Arrhenius-type, c) modified Hensel-Spittel model

Table 3: Comparison of constitutive models using AARE

Model	Strain rate (s^{-1})	Temperature (°C)						Average
		950	1000	1050	1100	1150	1200	
MJC	0.1	11.00	19.38	15.25	17.39	19.59	22.24	13.76
	1	2.30	8.45	11.70	12.46	16.19	23.19	
	10	10.68	7.54	13.56	11.38	13.29	18.66	
	50	11.09	9.38	5.74	8.87	15.24	25.71	
SA	0.1	2.92	9.41	6.91	13.24	21.07	34.18	9.78
	1	5.93	4.70	5.02	6.88	9.93	19.35	
	10	11.16	4.52	5.08	5.37	5.95	12.07	
	50	14.21	9.19	6.62	4.14	6.92	9.98	
MHS	0.1	7.80	9.64	9.18	8.46	9.52	10.02	11.25
	1	12.16	7.05	4.54	6.13	7.30	8.86	
	10	26.46	14.94	6.98	5.17	5.26	6.91	
	50	32.28	25.37	18.79	8.77	6.56	11.04	

model has a good prediction value only at the reference temperature and strain rate, as shown in **Figure 4**.

The value of R of the strain-compensated Arrhenius-type model is 0.9771, and the AARE values range from 2.92 to 34.18. **Table 2** shows that at a strain rate of 0.1 s^{-1}, the value of AARE at 950 °C is the lowest (2.92) and the highest at 1200 °C (34.18). The AARE values range from 4.14 to 19.35 at the other strain rates, and the average value of AARE is greatly reduced. The predicted values of the model under the 0.1 s^{-1} strain rate deviate from the test values, as shown in **Figure 5**.

The modified Hensel-Spittel model's value of R is 0.9334, and the AARE values range from 4.54 to 32.28. Taking the peak stress as the dividing line, as shown in **Figure 6**, the model prediction accuracy of the part after the peak stress of the rheological curve is high, but the prediction result of the part before the peak stress has a large error. It demonstrates that this model does not consider the strain adequately. However, the degree of curve position fitting under various temperatures is satisfactory.

Overall, the strain-compensated Arrhenius-type model accurately predicts the flow behavior of the N06625 nickel-based alloy at high temperatures over a wide temperature and strain-rate range. However, due to a large number of parameters and polynomial equations, this model takes a long time for the calculation.[12] It can be seen from **Figure 6** that the AARE increases sharply at 0.1 s^{-1} and 1200 °C. Before the peak stress, the modified Hensel-Spittel model is unable to accurately predict the part. As a result, this model can be chosen only when the portion of the flow curve after the peak stress is considered. Modeling under fewer deformation conditions is more accurate with the modified Johnson-Cook model.[11] The model's overall accuracy improves as deformation conditions decrease. A group calculation according to the deformation conditions and setting multiple reference conditions can also reduce the error.

In addition, except for ANN, there is almost no model that can accurately simulate the whole flow curve, but the ANN model cannot be combined with the finite-element software at present. This is because the flow stress is affected by the coupling of the temperature, strain rate and strain. Due to the nonlinear relationship between the flow stress and process parameters, it is difficult to establish a desirable constitutive equation, especially for describing the thermal deformation behavior of materials in a wide range of temperatures and strain rates. In recent years, some scholars have used the subsection method to establish an improved constitutive model. Mei[23] takes the peak stress as the dividing line, from zero to the peak stress as the first stage, fitting the

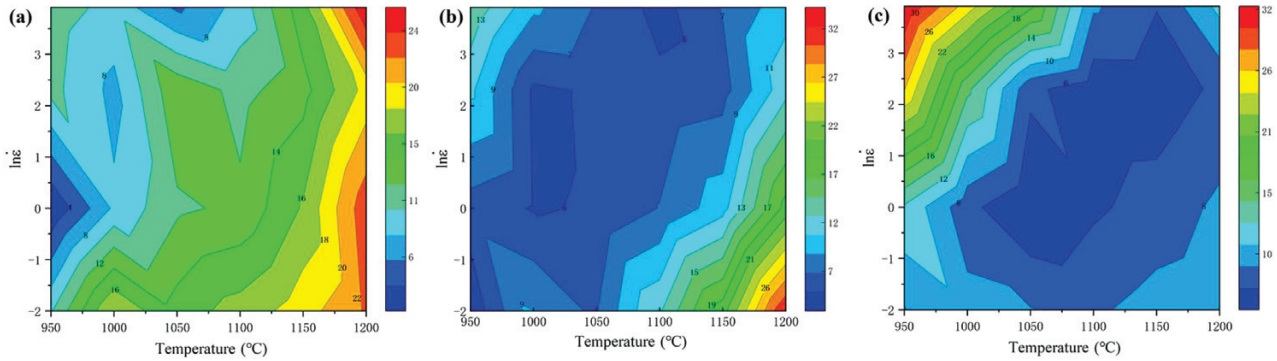

Figure 8: Comparison of the AARE for: a) modified Johnson-Cook, b) strain-compensated Arrhenius-type, c) modified Hensel-Spittel model

linear equation from the peak stress to the final stress as the second stage, and fitting the nonlinear equation. Liu[24] takes the work-hardening dynamic recovery stage as the first stage and the dynamic-recrystallization stage as the second stage, predicting the flow stress by combining the dynamic-recrystallization critical model and the dynamic model. Although the prediction accuracy of the segmented model has been improved, the complexity and time required for the calculation have also increased significantly. Therefore, it needs to be improved in the future.

4 CONCLUSIONS

A comparative study was carried out on the ability of the modified Johnson-Cook, strain-compensated Arrhenius-type and modified Hensel-Spittel constitutive models to describe the elevated-temperature flow behavior of a N06625 nickel-based alloy in a temperature range of 950–1200 °C at strain rates of 0.1–50 s^{-1}. Based on this study, the following conclusions can be drawn:

The true stress-strain curve was drawn based on the data from the thermal-compression simulation test. The original curve was modified to eliminate the influence of friction and adiabatic temperature rise. The errors before and after the flow stress correction cannot be neglected, especially at large strain rates.

A modified Johnson-Cook, strain-compensated Arrhenius-type and modified Hensel-Spittel constitutive models were obtained. The strain-compensated Arrhenius-type constitutive model can more accurately predict the high-temperature flow behavior of an entire machining area. The modified Johnson-Cook model has the highest accuracy when only one curve is predicted. The modified Hensel-Spittel model is more suitable for predicting the part after the peak stress of the curve.

The value of R of the modified Johnson-Cook model is 0.9533, and the AARE values are between 2.30 and 25.71. The value of R of the strain-compensated Arrhenius-type model is 0.9771, and the AARE values are between 2.92 and 34.18. The value of R of the modified Hensel-Spittel model is 0.9334, and the AARE values are between 4.54 and 32.28.

The strain-compensated Arrhenius-type constitutive model requires more calculations and time to obtain results than the other two models.

Acknowledgment

This project was supported by the Key Core Technology and Common Technology Research and Development Project of the Shanxi Province (20201102017), Excellent Innovation Project for Graduate Students from the Shanxi Province (2021Y666), and Key Special Project of "Science and Technology for Economy 2020" (2020YFF0405969).

5 REFERENCES

[1] S. Floreen, G. E. Fruchs, W. J. Yang, The Metallurgy of Alloy 625, Superalloys 718, 625, 706 and Various Derivatives, (**1994**), 13–37, doi:10.7449/1994/Superalloys_1994_13_37

[2] M. Sundararaman, P. Mukhopadhyay, S. Banerjee, Carbide precipitation in nickel base superalloys 718 and 625 and their effect on mechanical properties, Superalloys 718, 625, 706 and Various Derivatives, (**1997**), 367–378, doi:10.7449/1997/Superalloys_1997_367_378

[3] V. Shankar, K. Bhanu Sankara Rao, S. L. Mannan, Microstructure and mechanical properties of Inconel 625 superalloy, J. Nucl. Mater., 288 (**2001**) 2, 222–232, doi:10.1016/S0022-3115(00)00723-6

[4] J. Mittra, J. S. Dubey, S. Banerjee, Acoustic emission technique used for detecting early stages of precipitation during aging of Inconel 625, Scripta Materialia, 49 (**2003**) 12, 1209–1214, doi:10.1016/S1359-6462(03)00488-3

[5] G. P. Dinda, A. K. Dasgupta, J. Mazumder, Laser aided direct metal deposition of Inconel 625 superalloy: Microstructural evolution and thermal stability, Materials Science and Engineering: A, 509 (**2009**) 1, 98–104, doi:10.1016/j.msea.2009.01.009

[6] Y. C. Lin, X.-M. Chen, A critical review of experimental results and constitutive descriptions for metals and alloys in hot working, Mater. Design, 32 (**2011**) 4, 1733–1759, doi:10.1016/j.matdes.2010.11.048

[7] Y. C. Lin, D.-X. Wen, J. Deng, G. Liu, J. Chen, Constitutive models for high-temperature flow behaviors of a Ni-based superalloy, Mater. Design, 59 (**2014**), 115–123, doi:10.1016/j.matdes.2014.02.041

[8] C. A. Badrish, A. Morchhale, N. Kotkunde, S. Kumar Singh, Prediction of flow stress using integrated JC-ZA constitutive model for Inconel 625 alloy, Materials Today: Proceedings, 46 (**2021**), 9287–9290, doi:10.1016/j.matpr.2020.02.140

[9] A. K. Godasu, U. Prakash, S. Mula, Flow stress characteristics and microstructural evolution of cast superalloy 625 during hot deformation, J. Alloy. Compd., 844 (**2020**), doi:10.1016/j.jallcom.2020.156200

[10] A. K. Gupta, V. K. Anirudh, S. K. Singh, Constitutive models to predict flow stress in Austenitic Stainless Steel 316 at elevated temperatures, Mater. Design, 43 (**2013**), 410–418, doi:10.1016/j.matdes.2012.07.008

[11] C. Brown, T. McCarthy, K. Chadha, S. Rodrigues, C. Aranas, G. C. Saha, Constitutive modeling of the hot deformation behavior of CoCrFeMnNi high-entropy alloy, Materials Science and Engineering: A, 826 (**2021**), doi:10.1016/j.msea.2021.141940

[12] J. Cai, K. Wang, P. Zhai, F. Li, J. Yang, A Modified Johnson-Cook Constitutive Equation to Predict Hot Deformation Behavior of Ti-6Al-4V Alloy, J. Mater. Eng. Perform., 24 (**2015**) 1, 32–44, doi:10.1007/s11665-014-1243-x

[13] Y. Li, E. Onodera, A. Chiba, Friction Coefficient in Hot Compression of Cylindrical Sample, Materials Transactions, 51 (**2010**) 7, 1210–1215, doi:10.2320/matertrans.M2010056

[14] H. Monajati, A. K. Taheri, M. Jahazi, S. Yue, Deformation characteristics of isothermally forged UDIMET 720 nickel-base superalloy, Metallurgical and Materials Transactions A, 36 (**2005**) 4, 895–905, doi:10.1007/s11661-005-0284-z

[15] R. Ebrahimi, A. Najafizadeh, A new method for evaluation of friction in bulk metal forming, J. Mater. Process. Tech., 152 (**2004**) 2, 136–143, doi:10.1016/j.jmatprotec.2004.03.029

[16] R. L. Goetz, S. L. Semiatin, The adiabatic correction factor for deformation heating during the uniaxial compression test, J. Mater. Eng. Perform., 10 (**2001**) 6, 710–717, doi:10.1361/105994901770344593

[17] M. C. Mataya, V. E. Sackschewsky, Effect of internal heating during hot compression on the stress-strain behavior of alloy 304L, Metallurgical and Materials Transactions A, 25 (**1994**) 12, 2737, doi:10.1007/BF02649226

[18] Y. C. Lin, X.-M. Chen, G. Liu, A modified Johnson–Cook model for tensile behaviors of typical high-strength alloy steel, Materials Sci-

ence and Engineering: A, 527 (**2010**) 26, 6980–6986, doi:10.1016/j.msea.2010.07.061

[19] C. M. Sellars, W. J. McTegart, On the mechanism of hot deformation, Acta Metallurgica, 14 (**1966**), 1136–1138, doi:10.1016/0001-6160(66)90207-0

[20] S. Gourdet, F. Montheillet, An experimental study of the recrystallization mechanism during hot deformation of aluminium, Materials Science and Engineering: A, 283 (**2000**) 1, 274–288, doi:10.1016/S0921-5093(00)00733-4

[21] A. Hensel, T. Spittel, Kraft- und Arbeitsbedarf bildsamer Formgebungsverfahren, 1st Edition, 1978, Deutscher Verlag für Grundstoffindustrie

[22] S. Spigarelli, M. El Mehtedi, A new constitutive model for the plastic flow of metals at elevated temperatures, J. Mater. Eng. Perform., 23 (**2014**) 2, 658–665, doi:10.1007/s11665-013-0779-5

[23] R.-B. Mei, L. Bao, F. Huang, X. Zhang, X.-W. Qi, X.-H. Liu, Simulation of the flow behavior of AZ91 magnesium alloys at high deformation temperatures using a piecewise function of constitutive equations, Mechanics of Materials, 125 (**2018**), 110–120, doi:10.1016/j.mechmat.2018.07.011

[24] M. Liu, Q.-X. Ma, J.-B. Luo, Hot deformation behavior and a two-stage constitutive model of 20Mn5 solid steel ingot during hot compression, Materials, 11 (**2018**) 3, 434, doi:10.3390/ma11030434